HHS Public Access

Author manuscript

Cell Calcium. Author manuscript; available in PMC 2016 December 01.

Published in final edited form as:

Cell Calcium. 2015 December ; 58(6): 638–648. doi:10.1016/j.ceca.2015.10.003.

A comparison of fluorescent Ca^{2+} indicators for imaging local Ca^{2+} signals in cultured cells

Jeffrey T. Lock[a], **Ian Parker**[a,b], and **Ian F. Smith**[a]

Jeffrey T. Lock: lockj@uci.edu; Ian Parker: iparker@uci.edu; Ian F. Smith: ismith@uci.edu

[a]Department of Neurobiology and Behavior, University of California, Irvine, CA

[b]Department of Physiology and Biophysics, University of California, Irvine, CA

Abstract

Localized subcellular changes in Ca^{2+} serve as important cellular signaling elements, regulating processes as diverse as neuronal excitability and gene expression. Studies of cellular Ca^{2+} signaling have been greatly facilitated by the availability of fluorescent Ca^{2+} indicators. The respective merits of different indicators to monitor bulk changes in cellular Ca^{2+} levels have been widely evaluated, but a comprehensive comparison for their use in detecting and analyzing local, subcellular Ca^{2+} signals is lacking. Here, we evaluated several fluorescent Ca^{2+} indicators in the context of local Ca^{2+} signals (puffs) evoked by inositol 1,4,5-trisphosphate (IP_3) in cultured human neuroblastoma SH-SY5Y cells, using high-speed video-microscopy. Altogether, nine synthetic Ca^{2+} dyes (Fluo-4, Fluo-8, Fluo-8 high affinity, Fluo-8 low affinity, Oregon Green BAPTA-1, Cal-520, Rhod-4, Asante Calcium Red, and X-Rhod-1) and three genetically-encoded Ca^{2+}-indicators (GCaMP6-slow, -medium and -fast variants) were tested; criteria include the magnitude, kinetics, signal-to-noise ratio and detection efficiency of local Ca^{2+} puffs. Among these, we conclude that Cal-520 is the optimal indicator for detecting and faithfully tracking local events; that Rhod-4 is the red-emitting indicator of choice; and that none of the GCaMP6 variants are well suited for imaging subcellular Ca^{2+} signals.

Keywords

Calcium; Fluorescent indicators; Local calcium signals; Genetically encoded calcium indicators; GCaMP6

Correspondence to: Ian F. Smith, ismith@uci.edu.

Disclosures

All authors declare that they have no competing financial interests.

Author contributions

Conception and design of the research by I.P. and I.F.S. Data was collected by J.T.L and analyzed by J.T.L., I.P. and I.F.S. Manuscript was written by J.T.L, I.P. and I.F.S. All authors have read and approved the published manuscript.

1. Introduction

The calcium ion (Ca^{2+}) is a ubiquitous second messenger that regulates a multitude of different physiological pathways including, secretion, fertilization, gene transcription and apoptosis. This single element is able to regulate so many diverse functions because cells have developed an elaborate toolkit of Ca^{2+} channels, pumps, exchangers and buffering proteins that enable changes in cytosolic [Ca^{2+}] to be generated with precise control in magnitude, space and time [1]. An excellent example is seen in smooth muscle where transient, spatially restricted microdomains of Ca^{2+} promote relaxation by specifically activating plasmalemmal K^+ channels, whereas waves and global Ca^{2+} signals that engulf the whole cell cause contraction [2] [3]. Our understanding of cellular Ca^{2+} signals has largely derived from progressive improvements in fluorescent Ca^{2+} indicator probes, coupled with advances in optical imaging technology. Indeed, it is now possible to monitor Ca^{2+} flux through individual channels in intact cells with millisecond temporal fidelity and sub-micrometer spatial resolution [4, 5].

The ability to image cellular Ca^{2+} signals dates back to the initial development of small molecule fluorescent Ca^{2+} indicator dyes by Roger Tsien [6, 7], together with a strategy for facile loading of these indicators into intact cells via membrane-permeant ester forms [8]. These dyes consist of a Ca^{2+} chelating moiety conjugated to a fluorescence reporter. In the absence of Ca^{2+}, photo-induced electron transfer from the Ca^{2+} chelator quenches fluorescence of the conjugated fluorophore. As Ca^{2+} levels rise this phenomenon is inhibited, resulting in a change in fluorescence intensity or shift in spectral properties (change in peak excitation or emission wavelengths). The first widely used indicator, fura-2 displays a shift in excitation spectra with Ca^{2+}, enabling absolute calibration of [Ca^{2+}] in terms of the ratio of fluorescence emitted at two different excitation wavelengths. However, with the exception of the newly developed indicator Asante Calcium Red (ACR) [9], all available ratiometric probes require excitation by phototoxic UV wavelengths, and the need to alternate excitation or emission wavelengths (as is the case for fura-2 and indo-1, respectively) severely limits temporal resolution. Instead, most studies imaging rapid, subcellular Ca^{2+} transients have utilized single wavelength Ca^{2+} indicators such as Fluo-4 and Oregon Green BAPTA-1 (OGB1), which produce a change in fluorescence intensity with [Ca^{2+}] without any appreciable shifts in excitation or emission spectra. These indicator dyes are bright, exhibit large changes in fluorescence (30-fold or more) on binding Ca^{2+}, and can be normalized for factors such as differences in dye loading by calculating a ‘pseudo-ratio’ of fluorescence relative to that at the same location either at rest before stimulation or after raising cytosolic [Ca^{2+}] to saturating levels.

The single-wavelength indicators operate within the visible light spectrum, with the most popular and those available with the greatest range of affinities utilizing blue excitation and green emission. Recently, there has been increased interest in red-shifted indicators [10]. Longer wavelengths (red and near IR) have inherent advantages of reduced phototoxicity and scattering, and leave the short end of the visible spectrum available for applications including simultaneous use of green or yellow fluorescent protein tags and optogenetic control of membrane potential using channel rhodopsin. Red-emitting Ca^{2+} dyes conjugated to BAPTA such as rhod-2 have long been available, but their use for monitoring cytosolic

Ca^{2+} signals is hampered by their propensity to accumulate in mitochondria. Newer dyes such as Rhod-4 and ACR are reported to show improved properties. However, to date only a few reports have utilized these probes [9, 11–13].

In parallel to the use of small-molecule synthetic indicators, the past decade has seen significant advances in the development of genetically encoded fluorescent Ca^{2+} indicators (GECIs). This has been motivated in large part by their promise as *in vivo* sensors of neuronal activity, employing changes in cytosolic Ca^{2+} resulting from opening of voltage-gated Ca^{2+} channels as a surrogate readout of action potential spiking. For this purpose, GECIs have some major advantages over synthetic indicators. They can be incorporated into the genome of transgenic mice, obviating any need for loading with exogenous indicator and, in contrast to the indiscriminate uptake of membrane-permeant dye esters, can be targeted to distinct populations of cells and/or subcellular locations using cell specific promoters and targeting sequences. A currently popular GECI is the single-fluorophore sensor GCaMP, consisting of the circularly permuted green fluorescent protein (GFP) fused to the calmodulin (CaM) binding region of chicken myosin light kinase (M13) at its N terminus and to a vertebrate CaM at its C terminus. Binding of Ca^{2+} causes the M13 and CaM domains to interact, leading to an increase in fluorescence. Several iterations of the original GCaMP sensor [14] have now been developed, with the most recent, GCaMP6, yielding three variants (slow, medium and fast) which have been reported to outcompete synthetic indicator dyes in terms of their sensitivity and dynamic range [15]. Nevertheless, the requirements for detecting bulk neuronal signals arising from spike-evoked opening of voltage-gated Ca^{2+} channels differ appreciably from those for monitoring subcellular Ca^{2+} transients from individual and small clusters of Ca^{2+} channels. Most notably, bulk cytosolic $[Ca^{2+}]$ in neurons decays relatively slowly over tens or hundreds of ms [16], whereas local Ca^{2+} microdomains collapse much more rapidly [17].

Several studies have evaluated the ability of various GECIs to monitor Ca^{2+} activity in the cell body, spines and dendrites of neurons, but none have compared GECI responses to synthetic Ca^{2+} dyes in the context of subcellular changes in cytosolic $[Ca^{2+}]$ [15, 18–20]. An earlier report did present a systematic comparison of small-molecule indicators for visualizing IP_3-mediated, subcellular Ca^{2+} puffs [21]. However, that study utilized slow, confocal laser scanning microscopy, before the advent of approaches including total internal reflection (TIRF) microscopy and fast EMCCD and sCMOS cameras that have greatly improved the spatial and temporal resolution of local Ca^{2+} signals. Moreover, new indicator dyes have since become available with improved Ca^{2+} binding properties, enhanced fluorescence brightness, and extended spectral range. A more recent report assessed the utility of green-emitting dyes for detecting local Ca^{2+} transients in cardiomyocytes [22] but was limited in scope, focusing only on three, similar fluo indicators (fluo-2, -3, -4).

Motivated by recent developments in both small-molecule and protein-based fluorescent Ca^{2+} probes, we describe here a systematic study of different indicators to determine optimum choices for imaging IP_3-mediated local Ca^{2+} signals in cultured mammalian cells using high-speed (~420 frames per second) camera-based fluorescence microscopy. We tested six green-emitting (Fluo-4, Fluo-8, Fluo-8 high affinity, Fluo-8 low affinity, Oregon Green BAPTA-1, Cal-520) and three red-emitting (Rhod-4, X-Rhod-1, and Asante Calcium

Red) synthetic Ca^{2+} dyes; as well as the slow, medium and fast GCaMP6 variants. Among these, we find, Cal-520 is the optimal indicator for detecting and faithfully tracking local Ca^{2+} puffs; that Rhod-4 is the red-emitting indicator of choice; and that none of the GCaMP6 variants are well suited for imaging subcellular Ca^{2+} signals.

2. Methods

2.1. Cell culture

Human neuroblastoma SH-SY5Y cells (ATCC; #CRL-2266) were cultured on cell culture-grade plastic tissue flasks in a 1:1 mixture of Ham's F12 (Gibco; #11765) and Eagle's minimal essential media (Gibco; #12360) supplemented with 10% fetal bovine serum (Gibco; #26140-095), 1% nonessential amino acids (Gibco; #11140-050), and 1% penicillin-streptomycin (Gibco; #15070-063). Cells were maintained at 37°C in a humidified environment with 95% air and 5% CO_2. For experimentation, cells were harvested by incubation with 0.25% Trypsin-EDTA (Gibco; #25200-056) and sub-cultured (50,000 cells/ml) on 35 mm glass-bottom imaging dishes (MatTek; #P35-1.5-14-C) for 2–4 days prior to imaging.

2.2. Materials and reagents

We used acetoxymethyl (AM) ester forms of the following organic Ca^{2+}- dyes (suppliers and catalog numbers listed in parentheses): Cal-520 (AAT Bioquest #21130), Fluo-8 (AAT Bioquest #21083), Fluo-8 high affinity (AAT Bioquest #21091), Fluo-8 low affinity (AAT Bioquest #21097), Rhod-4 (AAT Bioquest #21122) ; Fluo-4 (Invitrogen #F-14201), Oregon Green BAPTA-1 (Invitrogen #O-6807), X-Rhod-1 (Invitrogen #X-14210); and Asante Calcium Red (TefLabs #3010). All dyes were reconstituted with dimethyl sulfoxide (DMSO) containing 20% pluronic F-127 (DMSO/F-127; Invitrogen; #P-3000MP) to a final concentration of 1 mM and were stored, shielded from light, at −20°C. The membrane-permeant caged IP_3 analogue ci-IP_3/PM [D-2,3-O-Isopropylidene-6-O-(2-nitro-4,5 dimethoxy) benzyl-myo-Inositol 1,4,5-trisphosphate Hexakis (propionoxymethyl) ester] was purchased from siChem (#cag-iso-2-145-10), solubilized with DMSO/F-127 to a final concentration of 200 μM and stored at −20°C. The GCaMP6 -slow, -medium, and -fast variants (plasmids #40753, #40754, and #40755, respectively) were obtained from Addgene. Lipofectamine 2000, for GCaMP6 induction, was purchased from Invitrogen (#11668030). All other reagents were purchased from Sigma-Aldrich.

2.3. Expression of GCAMP6 variants in SH-SY5Y cells

SH-SY5Y cells were sub-cultured in 60 mm culture-grade plastic dishes and transfected with either the slow, medium, or fast version of GCaMP6 using Lipofectamine 2000 according to the manufacturer's instruction for adherent cells. After 24 hrs, cells were transferred to 35 mm imaging dishes and used for experimentation 2–3 days post-transfection.

2.4. Ca^{2+} imaging

Cell culture medium was replaced with a Ca^{2+}-containing HEPES buffered salt solution (Ca^{2+}-HBSS) composed of (mM): 135 NaCl, 5.4 KCl, 2 $CaCl_2$, 1 $MgCl_2$, 10 HEPES, and 10

glucose; pH=7.4 set with NaOH at room temperature (RT)). Cells were then incubated with AM esters of 5 μM Fluo-4, Fluo-8, Fluo-8 high affinity, Fluo-8 low affinity, OGB1 Oregon Green BAPTA-1, Cal-520; or 2 μM Rhod-4, ACR, or X-Rhod-1; together with 1 μM ci-IP_3/PM for 1 hr at RT in Ca^{2+}-HBSS. A lower concentration of red-shifted dyes was used to avoid the potential for mitochondrial accumulation of these indicators [23]. Cells previously transfected to express GCaMP6-slow, -medium, or -fast sensors were incubated with 1 μM ci-IP_3/PM for 1 hr at RT in Ca^{2+}-HBSS. Following loading, cells were washed with Ca^{2+}-HBSS for 30 min prior to imaging.

Imaging of local cytosolic Ca^{2+} signals was accomplished using a home-built microscope system based around an Olympus IX 50 microscope equipped with an Olympus 60X TIRF objective (NA 1.45) described previously [5, 24]. Excitation light from the expanded beam of either 488 nm (Coherent), 532 nm (Coherent) or 561 nm (Opto-Engine) diode pumped solid-state (DPSS) lasers was introduced by a small reflective prism and brought to a focus at the rear focal plane of the objective. The laser spot was positioned near the center of the objective aperture, to create wide-field (WF) excitation. Emitted fluorescence was collected through the same objective and filtered by steep-cut long pass filters (Semrock) with cut-off wavelengths of 488 nm, 532 nm, or 568 nm corresponding to the respective laser wavelengths. Images were acquired using a Cascade 128+ electron-multiplied charged coupled device (EMCCD) camera (Roper Scientific) with 128 × 128 pixel resolution (1 pixel = 0.4 μm) at a rate of ~420 frames per sec (fps). UV light, introduced by a UV-reflecting dichroic in the light path was uniformly focused throughout the field of view to photo-release ci-IP_3, with the amount of ci-IP_3 released controlled by varying the flash duration (i.e. stimulus strength). UV light was obtained from a xenon arc illuminator and filtered through a 350–400 nm bandpass filter, with flash duration set by an electronically controlled shutter (UniBlitz). Image data were streamed to computer memory using MetaMorph software (Universal Imaging/Molecular Devices) and were subsequently stored on hard disc for offline analysis.

2.5. Image analysis

Image data in MetaMorph stk format were converted into tiff stacks and processed using a custom algorithm, written in the MatLab programming language, for the automated detection and analysis of local Ca^{2+} signals from fluorescence video recordings [25, 26]. Image stacks were processed by first subtracting the background fluorescence for the entire image stack, spatially smoothed with a Gaussian filter, and temporally smoothed with two Butterworth filters. Boxcar scans were used to detect local fluorescence transients and their x-y coordinates were determined as the centroid of a 2 dimensional Gaussian fitted to each event from the spatially and temporally filtered image stacks. Duplicate, false-positive, and incomplete events were manually excluded from further analysis. Event amplitudes were expressed as a fluorescence ratio ($\Delta F/F_0$) by taking the amplitude above baseline of the fitted Gaussian function at the time of peak fluorescence (ΔF) divided by the mean fluorescence (F_0) at that pixel averaged over 100 frames before stimulation. Event kinetics were characterized as $rise_{20\text{-}80}$ time (from 20% to 80% of peak amplitude) and $fall_{80\text{-}20}$ time (from 80% to 20 % of peak amplitude). We also determined the resting fluorescence (F_0; in arbitrary camera units) of cells loaded with each indicator under standard conditions (laser

angle and intensity, neutral density filter, camera gain); and the signal-to-noise (SNR) ratio of events.

3. Results and Discussion

3.1. Experimental procedure

Ca^{2+} puffs in response to photo-liberation of i-IP_3 were recorded using each Ca^{2+} indicator individually loaded into human neuroblastoma SH-SY5Y cells; a cell line well characterized for the study of local Ca^{2+} signals [5, 25, 27–29]. Puffs were evoked using photolysis flashes with a fixed intensity and duration (75 msec) selected to generate a measurable local response without producing a global rise in cytosolic [Ca^{2+}] that would obscure the detection and analysis of puffs. As described in section 2.5, we utilized a custom algorithm to automate detection and localization of puff sites and to quantify events arising at these sites Fig. 1A shows a representative imaging field of resting fluorescence of several SH-SY5Y cells loaded with the Ca^{2+} sensitive indicator Cal-520, onto which all detected puff site locations are mapped [25, 26]. Fluorescence traces monitored at these sites are shown in Fig. 1B, numbered as marked in Fig 1A, and an example of a single puff event is shown on expanded scales in Fig. 1C. The traces represent measurements of fluorescence intensity centered on located puff sites, weighted by a spatial Gaussian function with standard deviation of 800 nm (2 pixels). The algorithm reports parameters including amplitude (fluorescence increase as a ratio of resting fluorescence, $\Delta F/F_0$) and $rise_{20\text{-}80}$ and $fall_{80\text{-}20}$ times (i.e. the time to rise/fall between 20% and 80% of peak amplitude) that are exported to an Excel spreadsheet for further analysis. Owing to cytosolic diffusion of Ca^{2+} and Ca^{2+}-bound indicator, fluorescence signals spread appreciably (mean full width at half-maximal amplitude ~8.8 μm) from the sites of Ca^{2+} release, so that recordings at one site were often contaminated by bleed-through of signals arising from an adjacent site. Importantly, our algorithm discriminates between the true origin of a puff event versus Ca^{2+} diffusing into a region from a closely adjacent site [25]. This feature is well demonstrated by comparing traces from sites 1 and 2 in Fig. 1B, where the algorithm assigned the first three events as originating at site 2 (grey shading) with the final event at site 1.

3.2. Evaluation of fluorescein-based single wavelength indicators

We first compared green-emitting Ca^{2+} indicator dyes chosen with dissociation constants (as specified by the manufacturers) appropriate to detect small increases in [Ca^{2+}] above the resting level: Fluo-4, K_d 345 nM; Fluo-8, 389 nM; Fluo-8 high affinity (Fluo-8H), 232 nM; Oregon Green BAPTA-1 (OGB1), 170 nM; and Cal-520, 320 nM), together with the lower affinity version of Fluo-8 (Fluo-8L), K_d 1.86 μM. Imaging was performed in wide-field mode with identical parameters (including dye and ci-IP_3 loading conditions, photolysis flash strength, and laser, microscope and camera settings) to facilitate direct comparison between dyes.

Fig. 2A depicts representative Ca^{2+} puffs recorded using each of the six green-emitting indicators, after aligning to their peak times. The event amplitudes are conventionally expressed as a ratio relative to resting fluorescence ($\Delta F/F_0$), so as to normalize for factors including differences in dye loading between different cells. Mean values of F_0 are plotted in

Fig. 2B for each indicator. Values are reported in arbitrary camera units, but are directly comparable across all indicators. Resting fluorescence varied over a nearly 4-fold range, with Cal-520 and Fluo-4 showing the lowest values, and Fluo-8H the greatest. Fig. 2C shows mean measurements of fluorescence changes (ΔF), averaged across all events detected using each indicator. Mean puff amplitudes expressed in this way were closely similar across all indicators. However, because of the variation in resting fluorescence (F_0), the mean ratio fluorescence amplitudes ($\Delta F/F_0$) of puffs thus showed greater differences between indicators, with the smallest $\Delta F/F_0$ of 0.085 ± 0.01 (mean ± SEM) for Fluo-8H and the largest $\Delta F/F_0$ of 0.271 ± 0.02 for Cal-520.

An important factor in selecting an indicator is the signal-to-noise ratio (SNR) obtained in fluorescence recordings; that is to say, how well a given Ca^{2+} signal can be detected above baseline noise. The predominant noise source in these recordings is photon shot noise, the standard deviation of which increases proportional to the square root of mean intensity. Thus, an optimal indicator should display both a low resting fluorescence (i.e. low baseline noise) and a large increase in fluorescence on binding Ca^{2+} [17]. Concordant with this, measurements of mean SNR showed the highest value for Cal-520 and lowest for Fluo-8H (Fig. 2D).

As an additional measure of the ‘goodness’ of an indicator for resolving local events, we determined the mean numbers of events detected per cell per second (Fig. 2E). The mean number of events detected using Fluo-8H was markedly lower than for the other indicators which, with the exception of Fluo-8, all showed similar values. Assuming that the underlying mean frequency of events and the mean amount of Ca^{2+} liberated per event remain constant, we interpret the low detection efficiency of Fluo-8H to arise because events involving small Ca^{2+} release gave fluorescence signals too small to be detected by the algorithm. This is further illustrated in Fig. 2F, plotting the cumulative numbers of events detected by the different indicators as a function of event amplitude ($\Delta F/F_0$). No events were detected with fluorescence amplitudes below a $\Delta F/F_0$ of about 0.05, determined primarily by the threshold detection setting of the algorithm. Above this level, Cal-520 displayed the greatest dynamic range, reporting events of >0.6 $\Delta F/F_0$. In comparison, Fluo-8H showed a much smaller range, with maximal signals no more than about 0.2 $\Delta F/F_0$; the other indicators lay between these two extremes.

To then explore the kinetic responses of the indicators we determined $rise_{20\text{-}80}$ and $fall_{80\text{-}20}$ times of fluorescence signals (Figs. 2G, H). We assume that the indicator displaying the fastest kinetics will most faithfully report the kinetics of the underlying Ca^{2+} signal, which is expected to rise rapidly during the onset of puffs owing to regenerative recruitment of IP_3R channels, but to decline more slowly during the falling phase when channels shut and Ca^{2+} ions diffuse away and become sequestered [17]. In this respect, Cal-520 showed the fastest rise times of all the indicators with 50% of detected events having rise times ≤ 40 msec, whereas the corresponding value for Fluo-8H was ≤ 150 msec (Fig. 2G). Fall times showed much less variability between indicators, excepting OGB1 which registered the slowest fall time with 50% of events ≤ 300 msec, versus ≤ 200 msec for Cal-520 (Fig. 2H).

Overall, we conclude that Cal-520 is the best green-emitting dye among those tested for detecting and analyzing local Ca^{2+} signals.

3.3. Evaluation of red-emitting small molecule indicators

Red-shifted Ca^{2+} indicators have advantages including freeing-up shorter wavelengths (<550nm) for simultaneous use of green- or yellow-fluorescent proteins and optogenetic stimulation, as well as benefits in reduced light scattering and phototoxicity arising from longer excitation wavelengths. We thus evaluated the red-shifted indicators Rhod-4, ACR and X-Rhod-1 for monitoring local Ca^{2+} signals (Fig. 3). Rhod-4 and ACR have K_d values of 525 nM and 400 nM, respectively, with respective excitation maxima (530 nm, 540 nm) closely aligned with our 532 nm laser, whereas X-Rhod-1 (K_d 700 nM) has an excitation peak closer to 580 nm, which we excited using a 561 nm laser. Other than changes in laser wavelengths we used the same imaging paradigm as described for the green-emitting indicators to record Ca^{2+} puffs evoked by UV flash photolysis of ci-IP_3.

Representative Ca^{2+} puffs obtained from fluorescence traces ($\Delta F/F_0$) from cells loaded with each red indicator dye are depicted in Fig. 3A. Figs. 3B–H show data obtained using these indicators, measuring basal fluorescence (B), puff amplitude (C, F), SNR (D), cumulative numbers of detected events (E) and $rise_{20\text{-}80}$ and $fall_{80\text{-}20}$ times (G,H); all determined in the same way as in Fig. 2. Basal resting fluorescence F_0 was higher in Rhod-4-loaded cells (~550 A.U., Fig. 3B) in comparison to ACR-loaded cells (~400 A.U.), but we cannot compare this to X-Rhod-1-loaded cells because of the use of a different laser. Overall, we conclude that Rhod-4 is the optimal indicator among the three red indicators, yielding the largest puff signals ($\Delta F/F_0$ 0.362 ± 0.02, 0.299 ± 0.02 and 0.178 ± 0.01 for Rhod-4, ACR and X-Rhod-1, respectively); appreciably higher SNR (Fig. 3D), slightly greater number of detected events (Fig. 3E), larger dynamic range (Fig. 3F), and faster resolution of puff rise times (Fig. 3G).

3.4. Comparison of Cal-520 versus Rhod-4

Having concluded that Cal-520 and Rhod-4 are the optimal choices for imaging of local Ca^{2+} signals at, respectively, green and red emission wavelengths we were interested to do a head-to-head comparison between these two indicators under identical conditions. Data from Figs. 2 and 3 cannot be directly compared because, although internally consistent, experiments using green and red indicators were undertaken at different times utilizing different cultures of cells. We thus performed closely matched, parallel experiments to overcome this limitation (Fig. 4). Dishes of SH-SY5Y cells from the same culture were loaded at the same time by incubation with 5 μM Cal-520/AM or 2 μM Rhod-4/AM together with 1 μM ci-IP_3/PM for 60 min, followed by 30 min for de-esterification in Ca^{2+}-HBSS. Recordings and analysis were then performed in exactly the same way as for Figs. 2 and 3, excepting that we now studied three different photolysis flash strengths; a brief (25 msec) flash that evoked a mean of 0.29 events per second per cell in Cal-520-loaded cells, and flashes of twice and three times this duration.

To facilitate the comparison of multiple parameters evoked by these differing UV flashes, data were normalized with respect to the mean response evoked by the shortest (1X) flash in

Cal-520-loaded cells. As shown in Fig. 4A, fewer puffs were detected with Rhod-4 as compared to Cal-520 in response to the 1X flash, whereas with longer flash durations evoking a greater frequency of events the detection efficiencies became more similar between the two dyes. Mean event amplitudes ($\Delta F/F_0$) were closely matched for Cal-520 and Rhod-4 at all stimulus strengths and, consistent with previous findings [28], event amplitudes showed only a slight increase with increasing flash duration (Fig. 4B). Kinetic measurements of mean puff rise (Fig. 4C) and fall times (Fig. 4D) showed no appreciable differences between Cal-520 and Rhod-4. We obtained recordings for several hours after loading both these indicators, and found little evidence for sequestration into organelles or extrusion from the cell.

In most respects, Cal-520 and Rhod-4 performed about equally well for recording Ca^{2+} puffs, implying that the major factor in choosing between them simply comes down to choice of operating wavelengths. However, one difference is the much lower efficiency of Rhod-4 for detecting puffs evoked by weak photorelease of i-IP_3. This is difficult to explain on the basis that events involving smaller release of Ca^{2+} may have evoked Rhod-4 fluorescence signals below the detection threshold, because mean fluorescence amplitudes were only weakly dependent on flash strength. Instead, it may be that that the presence of Rhod-4 itself affected IP_3-mediated Ca^{2+} liberation.

3.5. Evaluation of genetically-encoded GCaMP6 indicators

The properties of genetically encoded Ca^{2+} indicator proteins have improved dramatically over recent years and the GCAMP6 family, developed in 2013, is reported to be more sensitive (in terms of their affinity for Ca^{2+}, kinetics and dynamic range) than their predecessors and to outperform OGB1 in detecting action potential-evoked Ca^{2+} signals in neurons [15]. We thus evaluated the three variants of GCaMP6 – slow (K_d 144 nM), medium (K_d 167 nM) and fast (K_d 375 nM)) – for their ability to detect and kinetically resolve local Ca^{2+} signals (Fig. 5).

GCaMP6 variants were transiently expressed in SH-SY5Y cells, loaded with ci-IP_3/PM for 60 min, and each evaluated under identical experimental conditions as described above for the organic dyes. All GCaMP6 probes displayed characteristic expression patterns of a cytosolic indicator with little evidence of intra-organellar localization (Supplementary Figure 1A). UV flash photolysis of ci-IP_3 produced repetitive localized fluorescence changes at discrete sites within GCaMP6 expressing cells, as illustrated in Fig. 5A for the slow, medium, and fast variants. All three GCaMPs showed a relatively rapid upstroke in fluorescence, comparable to signals generated by the organic indicator dyes but with a much slower decay phase. The mean basal fluorescence signal (F_0) was lower for GCaMP6-fast than for the other variants (Fig 5B), whereas mean peak amplitudes (ΔF) of local Ca^{2+} signals (Fig 5C) and SNRs (Fig 5D) were similar among all three GCaMPs. However, GCaMP6-fast did detect more events per cell per second as compared with the slow and medium variants (Fig. 5E), and showed a greater dynamic range (Fig. 5F) reporting events with amplitudes up to about 1.5 $\Delta F/F_0$ versus about 0.8 $\Delta F/F_0$ for GCaMP6-slow.

The greatest differences among the GCaMP6 variants were seen in their abilities to track rise and fall times of local events. Median $rise_{20\text{-}80}$ times of puffs recorded with slow,

medium and fast GCaMPs were, respectively, about 70, 120, and 160 msec (Fig. 5G). These values fall well within the range of the published rise times of the different GCaMP6 sensors [15] and likely reflect changes in the conformational state of the protein (and thus fluorescence) following Ca^{2+} binding rather than the 'true' kinetics of local [Ca^{2+}] increase, given that corresponding rise times with Cal-520 were about 40 msec. Median $fall_{80\text{-}20}$ times for slow, medium and fast GCaMP6 variants were about 900, 750 and 400 msec (Fig. 5H).

3.6. Comparison of Cal-520 versus GCaMP6-fast

Finally, we undertook a more detailed comparison of the best performing GCaMP6 indicator (the fast variant) with Cal-520, directly comparing responses to photoreleased i-IP3 in cells imaged on the same day, under identical conditions. Photolysis flashes of three durations (25, 50, and 75 ms; denoted as 1X, 2X and 3X) were used to photo-release corresponding amounts of $i\text{-}IP_3$ and evoke local Ca^{2+} signals (Figs. 6A, B). As previously demonstrated [28], the frequency of puffs recorded with Cal-520 increased with the flash duration (Fig. 6C), but their mean amplitudes showed little change (Fig. 6D). Moreover, the shorter (1X) flash usually evoked only localized puffs with little elevation of basal Ca^{2+}, whereas stronger flashes evoked puffs superimposed on a gradually rising global baseline (Fig. 6A). Recordings with GCaMP6-fast also showed an increase in puff frequency with increasing flash duration, but the numbers of events detected per cell were lower than with Cal-520 for all flash durations. (Figs. 6B, C). In contrast to the findings with Cal-520, mean puff amplitudes increased considerably with increasing flash duration (Fig. 6D), and even the strongest flash evoked no appreciable rise in global, basal Ca^{2+} (Fig. 6B).

The mean rise times of puffs recorded with GCaMP6-fast were about 3-times slower than recorded with Cal-520 for all flash durations (Fig. 6E). The mean fall times of puffs recorded with Cal-520 remained about constant (200 msec) for all flash durations, whereas fall times with GCaMP6-fast became longer with increasing flash duration. Beyond their poor kinetic resolution, these results raise further concerns for the use of GCaMPs for recording cellular Ca^{2+} signals in suggesting that they may perturb the underlying Ca^{2+} release process by reducing sensitivity to IP_3 and suppressing the global rise in basal Ca^{2+} at higher [IP_3]. To explore whether reducing the expression level of GCaMP6-fast could mitigate this, we compared puff properties between low-expressing cells with a resting fluorescence only just sufficient to locate cells and obtain satisfactory Ca^{2+} signals and cells exhibiting about 3-fold higher expression (Supplementary figure 1B). We did not find any significant differences in puff amplitudes, rise/fall times and event frequency between low- and high-expressing cells (Supplementary figure 1C–F).

3.7 Conclusion

An ideal fluorescent indicator for studying local Ca^{2+} signals will have low basal fluorescence (and hence a low level of photon shot noise) together with a large change in fluorescence in response to small changes in [Ca^{2+}], resulting in a good signal-to-noise ratio. Moreover, it should have fast Ca^{2+} binding and dissociation rates so as to faithfully report brief, transient changes in [Ca^{2+}]. Based on these criteria we evaluated several green and red-emitting Ca^{2+} sensitive fluorescent dyes and GCaMP6 fluorescent protein indicators for their abilities to monitor IP_3-evoked Ca^{2+} puffs in neuroblastoma cells. Although we have

reported that imaging of puffs is enhanced and facilitated by use of total internal reflection fluorescence (TIRF) microscopy together with cytosolic loading of the slow Ca^{2+} buffer EGTA [5, 29], we did not use those approaches here, preferring to simplify the conditions and avoid introducing additional variables which might be poorly controlled. We found that Cal-520 is our indicator of choice among the green-emitting small-molecule indicators tested, and that Rhod-4 is the best among the red indicators. Indeed, both perform similarly well, so that the choice between them may be made primarily on the basis of which excitation and emission wavelengths are most appropriate for a particular experiment. In comparison to our results with small-molecule synthetic Ca^{2+} indicators none of the GCaMP6 proteins performed well, exhibiting slower kinetic responses and lower efficiency in detecting events. Moreover, expression of GCaMP appeared to affect the sensitivity to IP_3, suggesting a possible perturbation of the underlying Ca^{2+} release mechanism. Thus, despite the advantages of GCaMPs for genetic expression and targeting, and their popularity as surrogates to monitor neuronal activity, we caution against extending the use of these fluorescent protein-based probes to investigate subcellular local Ca^{2+} signals.

Supplementary Material

Refer to Web version on PubMed Central for supplementary material.

Acknowledgments

The authors thank Kyle L. Ellefsen for assistance with the algorithm used to detect and analyze local Ca^{2+} signals. This work was supported by National Institutes of Health grants GM 100201 to I.F.S, and GM 048071 and GM 065830 to I.P.

References

1. Berridge MJ, Lipp P, Bootman MD. The versatility and universality of calcium signalling. Nat Rev Mol Cell Biol. 2000; 1:11–21. [PubMed: 11413485]
2. Hill-Eubanks DC, Werner ME, Heppner TJ, Nelson MT. Calcium signaling in smooth muscle. Cold Spring Harbor perspectives in biology. 2011; 3:a004549. [PubMed: 21709182]
3. Hagenston AM, Bading H. Calcium signaling in synapse-to-nucleus communication. Cold Spring Harbor perspectives in biology. 2011; 3:a004564. [PubMed: 21791697]
4. Demuro A, Parker I. Imaging the activity and localization of single voltage-gated Ca(2+) channels by total internal reflection fluorescence microscopy. Biophys J. 2004; 86:3250–3259. [PubMed: 15111438]
5. Smith IF, Parker I. Imaging the quantal substructure of single inositol trisphosphate receptor channel activity during calcium puffs in intact mammalian cells. Proc Natl Acad Sci U S A. 2009; 106:6404–6409. [PubMed: 19332787]
6. Minta A, Kao JP, Tsien RY. Fluorescent indicators for cytosolic calcium based on rhodamine and fluorescein chromophores. J Biol Chem. 1989; 264:8171–8178. [PubMed: 2498308]
7. Grynkiewicz G, Poenie M, Tsien RY. A new generation of calcium indicators with greatly improved fluorescence properties. J Biol Chem. 1985; 260:3440–3450. [PubMed: 3838314]
8. Tsien RY. A non-disruptive technique for loading calcium buffers and indicators into cells. Nature. 1981; 290:527–528. [PubMed: 7219539]
9. Hyrc KL, Minta A, Escamilla PR, Chan PP, Meshik XA, Goldberg MP. Synthesis and properties of Asante Calcium Red--a novel family of long excitation wavelength calcium indicators. Cell Calcium. 2013; 54:320–333. [PubMed: 24017967]

10. Oheim M, van ‘t Hoff M, Feltz A, Zamaleeva A, Mallet JM, Collot M. New red-fluorescent calcium indicators for optogenetics, photoactivation and multi-color imaging. Biochimica et biophysica acta. 2014; 1843:2284–2306. [PubMed: 24681159]
11. Ljubojevic S, Walther S, Asgarzoei M, Sedej S, Pieske B, Kockskamper J. In situ calibration of nucleoplasmic versus cytoplasmic Ca(2)+ concentration in adult cardiomyocytes. Biophys J. 2011; 100:2356–2366. [PubMed: 21575569]
12. Xie W, Santulli G, Guo X, Gao M, Chen BX, Marks AR. Imaging atrial arrhythmic intracellular calcium in intact heart. J Mol Cell Cardiol. 2013; 64:120–123. [PubMed: 24041536]
13. Iguchi M, Kato M, Nakai J, Takeda T, Matsumoto-Ida M, Kita T, Kimura T, Akao M. Direct monitoring of mitochondrial calcium levels in cultured cardiac myocytes using a novel fluorescent indicator protein, GCaMP2-mt. International journal of cardiology. 2012; 158:225–234. [PubMed: 21295866]
14. Nakai J, Ohkura M, Imoto K. A high signal-to-noise Ca(2+) probe composed of a single green fluorescent protein. Nature biotechnology. 2001; 19:137–141.
15. Chen TW, Wardill TJ, Sun Y, Pulver SR, Renninger SL, Baohan A, Schreiter ER, Kerr RA, Orger MB, Jayaraman V, Looger LL, Svoboda K, Kim DS. Ultrasensitive fluorescent proteins for imaging neuronal activity. Nature. 2013; 499:295–300. [PubMed: 23868258]
16. Ross WN, Manita S. Imaging calcium waves and sparks in central neurons. Cold Spring Harb Protoc. 2012; 2012:1087–1091. [PubMed: 23028073]
17. Shuai J, Parker I. Optical single-channel recording by imaging calcium flux through individual ion channels: theoretical considerations and limits to resolution. Cell Calcium. 2005; 37:283–299. [PubMed: 15755490]
18. Hendel T, Mank M, Schnell B, Griesbeck O, Borst A, Reiff DF. Fluorescence changes of genetic calcium indicators and OGB-1 correlated with neural activity and calcium in vivo and in vitro. J Neurosci. 2008; 28:7399–7411. [PubMed: 18632944]
19. Mao T, O’Connor DH, Scheuss V, Nakai J, Svoboda K. Characterization and subcellular targeting of GCaMP-type genetically-encoded calcium indicators. PLoS One. 2008; 3:e1796. [PubMed: 18350138]
20. Ohkura M, Matsuzaki M, Kasai H, Imoto K, Nakai J. Genetically encoded bright Ca2+ probe applicable for dynamic Ca2+ imaging of dendritic spines. Anal Chem. 2005; 77:5861–5869. [PubMed: 16159115]
21. Thomas D, Tovey SC, Collins TJ, Bootman MD, Berridge MJ, Lipp P. A comparison of fluorescent Ca2+ indicator properties and their use in measuring elementary and global Ca2+ signals. Cell Calcium. 2000; 28:213–223. [PubMed: 11032777]
22. Hagen BM, Boyman L, Kao JP, Lederer WJ. A comparative assessment of fluo Ca2+ indicators in rat ventricular myocytes. Cell Calcium. 2012; 52:170–181. [PubMed: 22721780]
23. Paredes RM, Etzler JC, Watts LT, Zheng W, Lechleiter JD. Chemical calcium indicators. Methods. 2008; 46:143–151. [PubMed: 18929663]
24. Demuro A, Parker I. “Optical patch-clamping”: single-channel recording by imaging calcium flux through individual muscle acetylcholine receptor channels. J Gen Physiol. 2005; 126:179–192. [PubMed: 16103278]
25. Ellefson KS, Parker B, Smith I, IF. An algorithm for automated detection, localization and measurement of local calcium signals from camera-based imaging. Cell Calcium. 201410.1016/j.ceca.2014.1006.1003
26. Lock JT, Ellefsen KL, Settle B, Parker I, Smith IF. Imaging local Ca2+ signals in cultured mammalian cells. Journal of visualized experiments : JoVE. 2015
27. Dickinson GD, Swaminathan D, Parker I. The probability of triggering calcium puffs is linearly related to the number of inositol trisphosphate receptors in a cluster. Biophys J. 2012; 102:1826–1836. [PubMed: 22768938]
28. Smith IF, Wiltgen SM, Parker I. Localization of puff sites adjacent to the plasma membrane: Functional and spatial characterization of calcium signaling in SH-SY5Y cells utilizing membrane-permeant caged inositol trisphosphate. Cell Calcium. 2009; 45:65–76. [PubMed: 18639334]

29. Smith IF, Wiltgen SM, Shuai J, Parker I. Calcium puffs originate from preestablished stable clusters of inositol trisphosphate receptors. Sci Signal. 2009; 2:ra77. [PubMed: 19934435]

- We evaluated multiple Ca^{2+} sensitive dyes to image local Ca^{2+} signals
- Cal-520 is the best performing green-emitting dye
- Rhod-4 is the best performing red-emitting dye
- GCaMP6 protein sensors are not suitable for imaging local Ca^{2+} signals

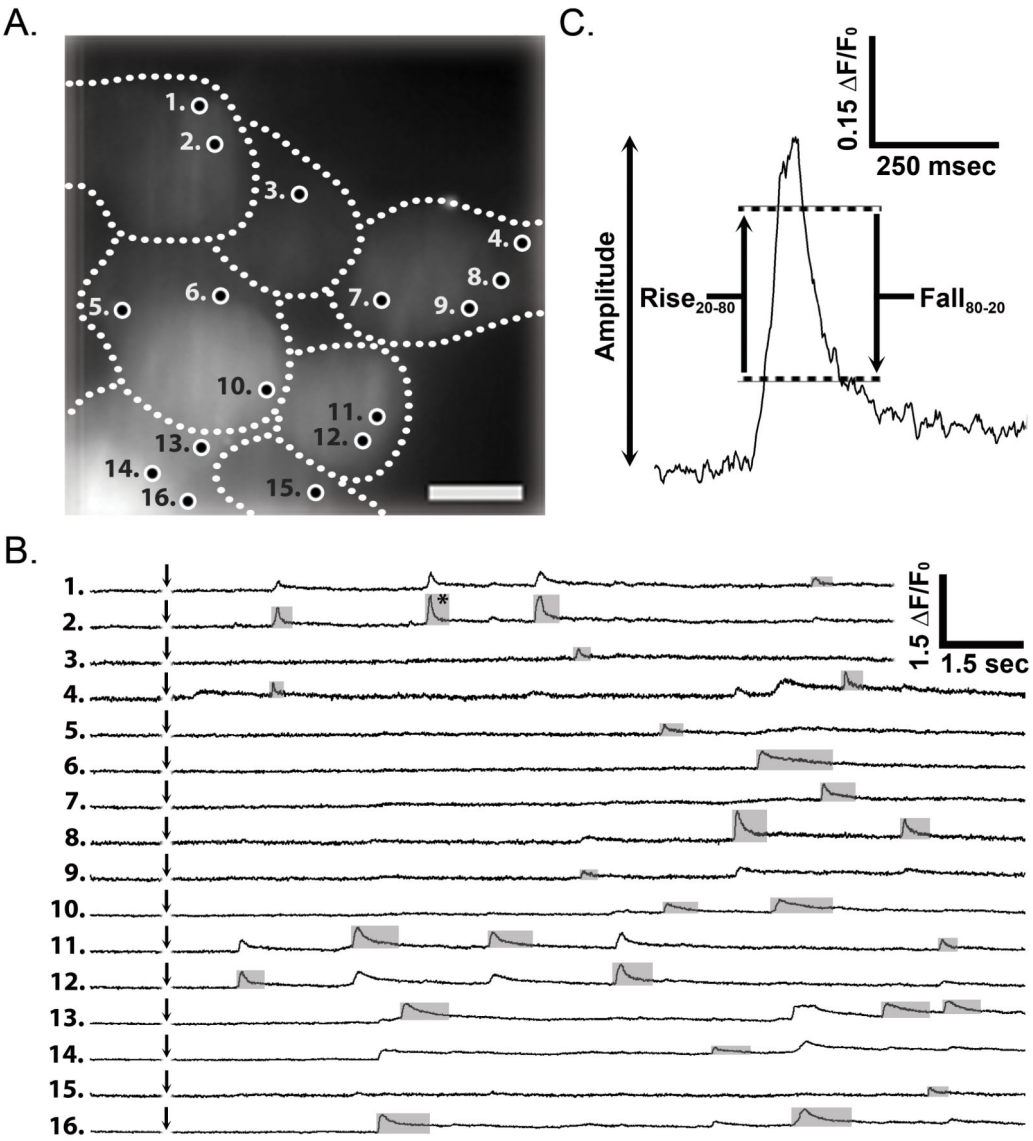

Fig. 1.

Experimental protocol for imaging local Ca^{2+} puffs evoked in SH-SY5Y cells by photorelease of iIP_3. (A) Resting fluorescence of several cells (outlined) which were loaded with Cal-520 and caged iIP_3. Circles mark sites at which puffs were observed following photorelease of iIP_3. Scale bar = 10 μm. (B) Traces depict simultaneous measurement of Cal-520 fluorescence over time ($\Delta F/F_0$) from the numbered sites in panel (A). A flash of UV light (75 ms duration) was delivered uniformly throughout the imaging field when marked by the arrows. Traces are scaled as the change in fluorescence (ΔF) divided by the resting fluorescence (F_0) at that site before stimulation, and were derived using an automated algorithm to identify the site of origin of each event (marked by grey boxes). (C) A single Ca^{2+} puff (identified by an asterisk in B) shown on expanded scales to illustrate measurements of amplitude and rise and fall times.

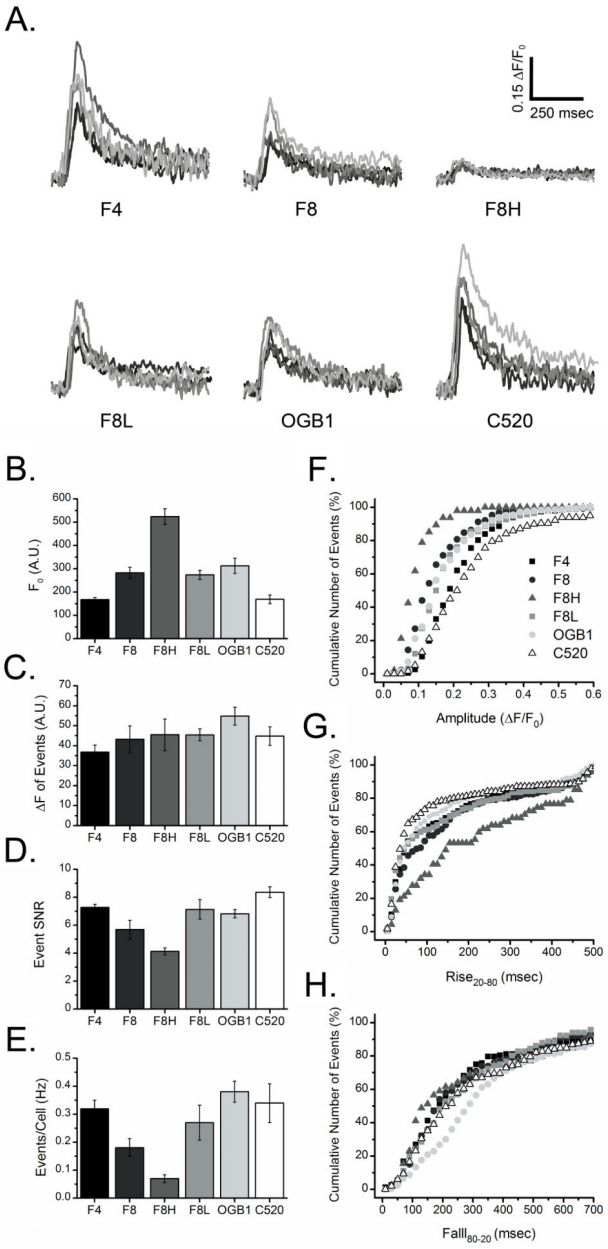

Fig. 2.

Analysis of local Ca^{2+} puffs imaged by by green-emitting fluorescent Ca^{2+} indicator dyes. (A) Representative traces showing Ca^{2+} puffs recorded using different indicators; Fluo-4 (F4), Fluo-8 (F8), Fluo-8 high affinity (F8H), Fluo-8 low affinity (F8L), Oregon Green BAPTA-1 (OGB1), and Cal-520 (C520). Fluorescence signals are scaled as $\Delta F/F_0$, and superimposed traces are aligned to their peak time and depicted in different shades of grey for clarity. All events were evoked by photorelease of iIP_3 under identical stimulus and recording conditions. Bar graphs (B–C) show measurements for each indicator of ; (B) background resting cell fluorescence (F_0) in arbitrary camera units (A.U), (C) peak amplitudes of puffs (ΔF), (D) signal-to-noise ratio (SNR) of puffs, and (E) the number of puffs detected per cell per second. Mean values were calculated for all cells and puffs within

a given imaging field (trial), and bars show mean ± 1 SEM from 6 trials for each indicator (F–G) Cumulative probability plots showing, for each indicator (depicted by different symbols), the percentage of all detected events as functions of ; (F) puff amplitude ($\Delta F/F_0$), (G) puff rise time ($rise_{20\text{-}80}$), and (H) fall time ($fall_{80\text{-}20}$). Total numbers of events analyzed for each parameter were at least 145 (Fluo-4), 100 (Fluo-8), 39 (Fluo-8H), 115-(Fluo-8L), 239 (OGB1), and 150 (Cal-520) ; in some instances signals were too small to obtain reliable measurements of fall time.

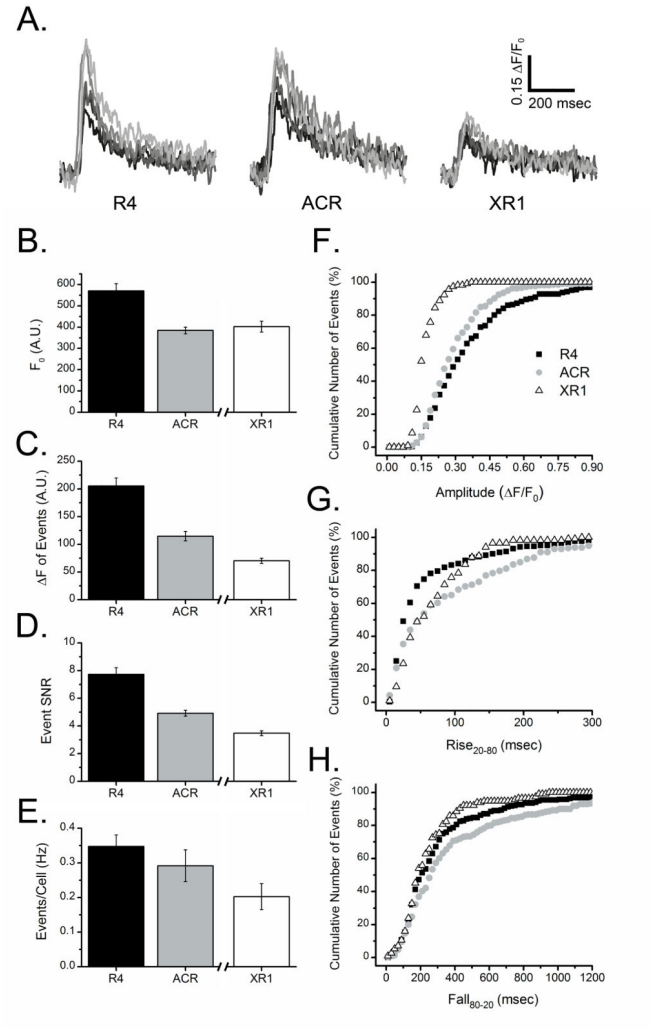

Fig. 3.

Analysis of local Ca^{2+} puffs imaged by red-emitting fluorescent Ca^{2+} indicator dyes; Rhod-4 (R4), Asante Calcium Red (ACR) and X-Rhod-1 (XR1). Each indicator was individually evaluated under identical conditions in SH-SY5Y cells, with the exception that Rhod-4 and ACR were excited with a 532 nm laser whereas X-Rhod-1 was excited with a 561 nm laser. For this reason, measurements of resting fluorescence of X-Rhod-1 (F_0, panel B) cannot be directly compared with the other two indicators. Otherwise, results are presented in the same way as Fig. 2. Data in (B–E) are expressed as the mean SEM from 8 trials for each indicator. Total numbers of events in cumulative probability graphs (F–H) are at least 215 (Rhod-4), 211 (Asante Calcium Red), and 113 (X-Rhod-1).

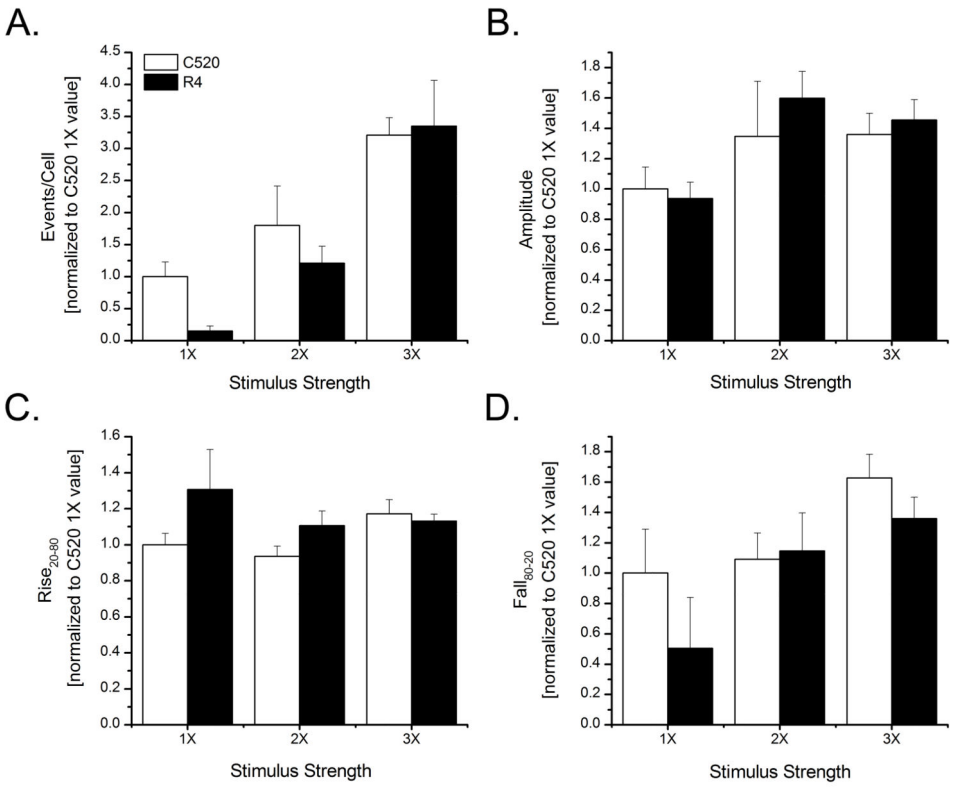

Fig. 4.

Head-to-head comparison of Cal-520 versus Rhod-4 for detecting and measuring Ca^{2+} puffs evoked by varying amounts of photoreleased iIP_3. UV photolysis flashes were of constant intensity and durations of 25 ms (1X), 50 ms (2X) and 75 ms (3X). Bar graphs show mean numbers of events evoked per cell per second (A), mean puff amplitudes (B), mean puff rise time (C) and mean puff fall time (D) of local Ca^{2+} signals detected by Cal-520 (open bars) and Rhod-4 (filled bars) in response to the different stimuli. All data are shown normalized relative to the mean values obtained using Cal-520 with the 1X flash duration. A range of 98–99 (1X), 172–178 (2X), and 271–287 (3X) local events for C520 and 7–8 (1X), 115–117 (2X), and 415–428 (3X) for R4 were analyzed from 3–6 experiments for each stimulus strength. Values were normalized to the mean Cal520 1X value for each parameter and are presented as mean ± 1 SEM.

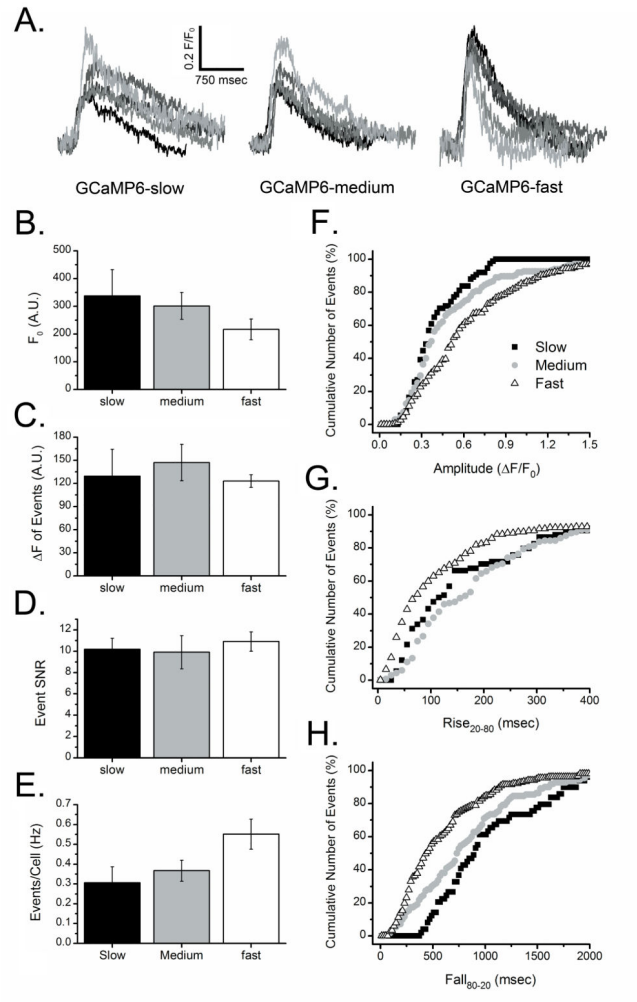

Fig. 5.

Recording local Ca^{2+} signals with genetically-encoded GCaMP6 indicators. Slow, medium and fast variants of GCaMP6 were individually expressed in SH-SY5Y cells, which were then loaded with ci-IP_3/PM and evaluated under identical conditions as described for the organic Ca^{2+} dyes. Results in (A–H) are presented in the same way as for Fig. 2. Data in (B–E) are expressed as the mean ± SEM from 6 trials for each GCaMP. Total numbers of events in cumulative probability graphs (F–H) are >52 (GCaMP6 slow), >110 (medium), and >150 (fast).

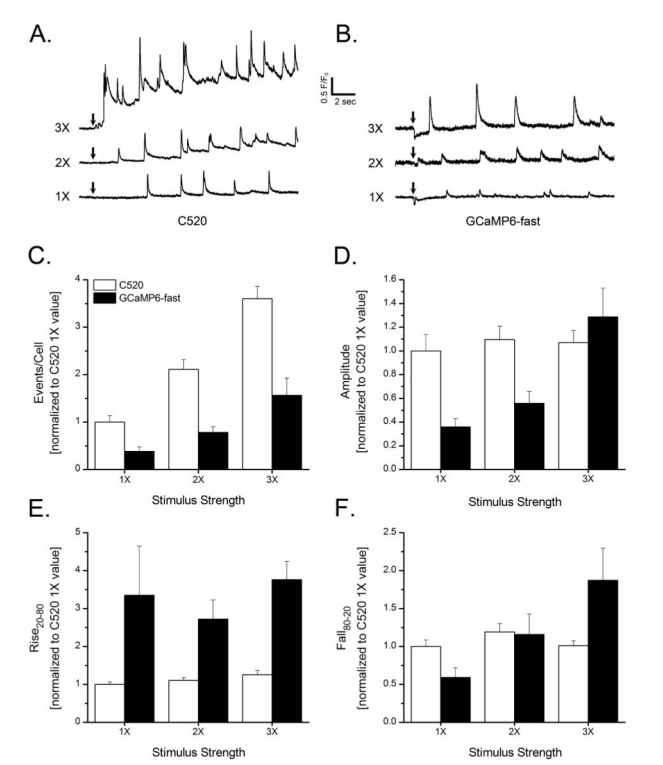

Fig. 6.

Head-to-head comparison of Cal-520 versus GCaMP6-fast for detecting and measuring Ca^{2+} puffs evoked by varying amounts of photoreleased iIP_3. (A,B) Representative traces showing local Ca^{2+} signals evoked by UV photolysis flashes of constant intensity and varying durations of 25 ms (1X), 50 ms (2X) and 75 ms (3X) recorded, respectively, using Cal520 and GCaMP6-fast. Transient downward deflections in the GCaMP traces likely reflect photobleaching by the UV flashes. (C–F) Bar graphs show mean numbers of events evoked per cell per second (C), mean puff amplitudes (D), mean puff rise time (E) and mean puff fall time (F) of local Ca^{2+} signals detected by Cal-520 (open bars) and GCaMP6-fast (filled bars) in response to the different stimuli. All data are shown normalized relative to the mean values obtained using Cal-520 with the 1X flash duration. Measurements with Cal-520 were made from at least 175 (1X flash), 327 (2X), and 258 (3X) local events; and for GCaMP6-fast from at least 23 (1X), 62 (2X), and 105 (3X) events.